EDGE ARTICLE

Check for updates

All publication charges for this article have been paid for by the Royal Society of Chemistry

Experimental evidence that halogen bonding catalyzes the heterogeneous chlorination of alkenes in submicron liquid droplets†

Meirong Zeng and Kevin R. Wilson [ID] *

A key challenge in predicting the multiphase chemistry of aerosols and droplets is connecting reaction probabilities, observed in an experiment, with the kinetics of individual elementary steps that control the chemistry that occurs across a gas/liquid interface. Here we report evidence that oxygenated molecules accelerate the heterogeneous reaction rate of chlorine gas with an alkene (squalene, Sqe) in submicron droplets. The effective reaction probability for Sqe is sensitive to both the aerosol composition and gas phase environment. In binary aerosol mixtures with 2-decyl-1-tetradecanol, linoleic acid and oleic acid, Sqe reacts 12–23× more rapidly than in a pure aerosol. In contrast, the reactivity of Sqe is diminished by 3× when mixed with an alkane. Additionally, small oxygenated molecules in the gas phase (water, ethanol, acetone, and acetic acid) accelerate (up to 10×) the heterogeneous chlorination rate of Sqe. The overall reaction mechanism is not altered by the presence of these aerosol and gas phase additives, suggesting instead that they act as catalysts. Since the largest rate acceleration occurs in the presence of oxygenated molecules, we conclude that halogen bonding enhances reactivity by slowing the desorption kinetics of Cl$_2$ at the interface, in a way that is analogous to decreasing temperature. These results highlight the importance of relatively weak interactions in controlling the speed of multiphase reactions important for atmospheric and indoor environments.

Introduction

The reaction rate of a gas phase molecule with an aerosol or droplet surface is governed by a set of kinetic steps that include adsorption/desorption, solvation/de-solvation, and diffusion.[1–5] The relative rates and coupling of these steps can often yield new pathways or catalytic mechanisms,[6–13] which are largely absent for a reaction occurring solely within a single phase. Given the central role that aerosols play in air pollution,[14,15] climate[16–18] and human health,[19] developing better insight, using laboratory measurements,[20] into the molecular factors that enhance, suppress or even catalyze multiphase chemical reactions is an important challenge. Using a model reaction, the heterogeneous chlorination of an alkene, we examine how "spectator molecules" in the gas and condensed phase decelerate as well as catalyze heterogeneous transformations. These results suggest that weak interactions, such as halogen bonding, can play substantial roles in controlling the speed at which multiphase transformations occur in the atmosphere and on indoor surfaces.[21–25]

Chemical Sciences Division, Lawrence Berkeley National Laboratory, Berkeley, CA 94720, USA. E-mail: krwilson@lbl.gov

† Electronic supplementary information (ESI) available. See DOI: 10.1039/d1sc02662c

Rudich and co-workers[6] observed that classes of chemical reactions that occur slowly in the gas phase ($k < 10^{-15}$ cm^3 molecules^{-1} s^{-1}), due to high activation barriers, are enhanced at monolayer organic surfaces that mimic tropospheric aerosol; in some cases by many orders of magnitude. For example, the reaction of bromine atoms with saturated aliphatic films occurs 10 000 times faster than predictions based upon analogous reactions in the gas phase. Conversely, gas phase reactions that are already fast[6] ($k \sim 10^{-12}$ cm^3 molecules^{-1} s^{-1}), exhibit only minimal surface enhancement.

Some fraction[26] of the enhanced reactivity at surfaces *vs.* the gas phase can be explained, somewhat trivially, by secondary reactions (*i.e.* promoted by the higher molecular densities at surfaces) or by the asymmetry of interfaces, where unreactive forward scattering trajectories yield additional possibilities for a reaction while in the gas phase they do not. More interestingly, surface enhancement factors are also consistent with well-known changes in the activation energy for an interfacial reaction, which are controlled by an array of interactions, such as molecular orientation, partial solvation, and the formation of unique interfacial complexes.[27] Theoretical work has also shown the importance of relatively weak interactions, such as hydrogen bonding, in governing reaction mechanisms at the surface of atmospheric droplets.[8–10] A recent study[11] revealed the importance of halogen bonded complexes in mediating iodine reactions at droplet surfaces. In most cases, a halogen bond is

weaker than a hydrogen-bond with typical bond lengths $\sim$2.8 Å, which form between an electrophilic molecule containing a halogen atom X (X = I, Br, Cl and F), and a nucleophilic molecule containing atoms, such as N, O, S etc.[28–32]

The reaction of Cl_2 with an alkene is relatively slow, so it is an ideal system to examine how the competing kinetics of chlorine adsorption/desorption, solvation/desolvation influence heterogeneous reaction rates. Here we examine the heterogeneous reaction of Cl_2 with squalene (Sqe) – a branched hydrocarbon with six C=C bonds. This reaction has been previously well-characterized by Popolan et al.[33] These prior results are leveraged to examine how the heterogeneous reaction rate depends upon temperature and the presence of small spectator molecules in the gas, which are unreactive towards Cl_2 (water, ethanol, acetone, and acetic acid). We also examine how doping a fatty acid, an ester, alcohol, or an alkane together with squalene in the aerosol phase alters its reactivity towards Cl_2. The chemistry examined in these model systems addresses the growing interest in understanding surface reaction mechanisms of unsaturated fatty acids and Sqe; major constituents of skin lipids[34] that are reactive towards halogens commonly released during indoor activities, e.g. bleach cleaning ([Cl_2] $\sim$ 100 ppb).[25,35–39]

This paper is organized as follows. The apparatus and experimental approach for quantifying heterogeneous chlorination rates, reaction products as well as determining effective uptake coefficients are described in Experimental design. Data is presented in Results and discussion aimed at understanding the changes in Sqe reactivity and product formation kinetics as a function of temperature and in binary mixtures of Sqe with 2-decyl-1-tetradecanol, oleic and linoleic acids, bis(2-ethylhexyl) sebacate and squalane. Additional results are presented examining how the reaction rate of Sqe is altered by the presence of small gas phase molecules such as H_2O, acetone, acetic acid, and ethanol. Together these experiments point to the interactions of Cl_2 with alkene (C=C), alcohol (–OH), acid (–COOH), and ester (–COOC) functional groups, which, like temperature, appear to modify the desorption kinetics of Cl_2 from the aerosol surface.

Experimental design

The heterogeneous reactions are conducted in the flowtube reactor, which has been widely used to explore the chemical kinetics of the heterogeneous reactions between aerosols and gases. Below we summarize the main features of the experiment.

Aerosol generation

Polydisperse aerosols are generated via homogeneous nucleation by passing dry N_2 (0.3 SLM) through a Pyrex tube located in a tube furnace. The Pyrex tube is filled with either a neat liquid (e.g. Sqe), or is mixed with an additive, i.e. linoleic acid (LA), oleic acid (OA), 2-decyl-1-tetradecanol ($C_{24}OH$), squalane (Sqa) or bis(2-ethylhexyl) sebacate (BES). These particular additives were selected because they are liquids at room

temperature and should be fully miscible in Sqe. Specifically, 2-decyl-1-tetradecanol, also a liquid at room temperature, is used rather than a normal alcohol to avoid the potential complications of well-known surface freezing effects, which can produce unexpected reaction products as observed for the OH oxidation of n-octacosane.[40] The final composition of the aerosol is assumed to identical to the composition of the liquid mixture prior to nucleating the aerosol. These chemicals were purchased from Sigma-Aldrich. As the vapor cools and exits the Pyrex tube, aerosols homogeneously nucleate. The aerosol-laden flow is then passed through an annular activated charcoal denuder to remove any residual gas-phase organics produced in the oven. The furnace temperature is adjusted for each experiment to generate stable aerosol streams. The average aerosol distribution is log-normal with a mass concentration of $\sim$3000 μg m^{-3} (2.0 × 10^6 cm^{-3}) and an average diameter of 150 nm.

Flowtube reactor

Upon exiting from the charcoal denuder, the aerosol flow is mixed with additional gases: Cl_2, O_2, wet or dry N_2 and for selected experiments gas phase additives (acetone, acetic acid, ethanol), to yield a total flow of 1.1 SLM. This flow is then introduced into the room temperature flowtube reactor (140 cm long and 2.5 cm inner diameter) that has, under these flow conditions, an average residence time of $\sim$37 seconds. For the temperature dependent experiments, a second double-walled flowtube reactor is used. This flow tube is 110 cm long with an inner diameter of 2.2 cm and an average residence time, at 1.1 SLM, of $\sim$23 seconds. Water is circulated in the outer portion of the flow tube in order to control reaction temperature. The recirculated water is fixed at 5, 25, 35 or 50 °C for the temperature dependent studies. Cl_2 is delivered from a standard cylinder (52 ppm balanced with nitrogen) purchased from Praxair, Inc. All experiments are conducted at atmospheric pressure and in the dark to avoid the possible photolysis of Cl_2 to produce Cl atoms.

Detectors

The aerosol chemical composition and its size distribution are measured in real time. The aerosol size distribution is measured by a TSI scanning mobility particle sizer (SMPS), consisting of a 3080L Differential Mobility Analyzer (DMA) and 3025 Condensation Particle Counter (CPC). The average size of the aerosol remains unchanged during reaction, which indicates that C–C bond scission pathways to produce volatile reaction products are unlikely.

The chemical composition of the aerosol is measured by a vacuum ultraviolet aerosol mass spectrometer (VUV-AMS),[41,42] located at the Chemical Dynamics Beamline 9.0.2, Advanced Light Source (ALS), Lawrence Berkeley National Laboratory, Berkeley, CA, USA. Mass spectra are recorded by first vaporizing the aerosol at $\sim$125 °C, followed by photoionization using tunable vacuum ultraviolet (VUV) light. Photon energies are selected for each experiment to minimize ion fragmentation. 9.6 eV is used for neat Sqe, while slightly larger energies are

used for Sqe/additive mixtures (*e.g.* 10.2 eV for Sqe/C$_{24}$OH mixture experiment).

Data analysis

In a typical experiment, a series of mass spectra are recorded as a function of Cl$_2$ exposure ([Cl$_2$] × reaction time) to obtain the kinetic decay of Sqe and the rise of reaction products, as shown in Fig. 1A. A plot of the normalized Sqe signal *versus* Cl$_2$ exposure is then fit to an exponential function to obtain a second order heterogeneous rate coefficient, k_{fit}.[43] k_{fit} is then used to compute an effective reaction probability for Sqe (γ_{eff}^{Sqe}) using,

$$\gamma_{eff}^{Sqe} = \frac{4k_{fit}D\rho N_A x_{Sqe}}{6cM} \quad (1)$$

where D, ρ, c, M and N_A are the average diameter, the initial particle density, velocity of Cl$_2$ gas, molecular weight of Sqe, and Avogadro's number, respectively. γ_{eff}^{Sqe} is the fraction of Cl$_2$ collisions with Sqe in the aerosol that yield a reaction.[43] For the mixture experiments, the mole fraction of the Sqe (x_{Sqe}) is used when computing γ_{eff}^{Sqe}. This approach allows us to focus on how the inherent reaction rate (*i.e.* γ_{eff}^{Sqe}) of Sqe with Cl$_2$ is altered in the presence of spectator molecules doped either together with Sqe in the aerosol phase or introduced as gases into the reactor.

A sequence of chlorinated reaction products (denoted SqeCl$_n$) are observed in the mass spectra and provide insight into the reaction mechanism shown in Fig. 1. It is difficult to obtain the absolute concentrations of the reaction products from the ion signal alone, due to the lack of absolute photo-ionization cross-sections and authentic standards to account for ion fragmentation patterns. Instead, the relative abundance (%) of the products are reported by normalizing the product signals (*e.g.* product [SqeCl$_n$]) to the initial signal of the unreacted Sqe (*e.g.* [Sqe]$_0$), namely [SqeCl$_n$]/[Sqe]$_0$.

Results and discussion

(a) Kinetics and temperature dependence of the heterogeneous reaction of neat Sqe

Fig. 1A shows the normalized decay of Sqe as a function of Cl$_2$ exposure, which when fit to an exponential function yields $\gamma_{eff}^{Sqe} = 3.5 \times 10^{-5}$ using eqn (1). This value is slightly smaller than previously reported value by Popolan *et al.*[33] (*i.e.* 6.6×10^{-5}). The reason for this difference is unclear, but likely reflects, as will be shown below, the sensitivity of this reaction to the presence of gas and particle phase species present in the reactor. Fig. 1B shows a difference mass spectrum (reacted–unreacted) showing reaction products; denoted SqeCl$_n$. This pattern of reaction products is consistent with the sequential electrophilic addition of Cl$_2$ to each of the 6 C=C bonds (Fig. 1C), after accounting for –(HCl)$_n$ elimination produced by dissociative photoionization as shown previously.[33,44] For example, the first-generation neutral product SqeCl$_2$ (C$_{30}$H$_{50}$Cl$_2$) appears at a m/z corresponding to either SqeCl (C$_{30}$H$_{49}$Cl) or Sqe-2 (C$_{30}$H$_{48}$) after one or two –HCl eliminations, respectively. This pattern is also consistent with –(HI)$_n$ elimination observed during dissociative photoionization of iodo-hydrocarbons.[45]

The kinetic evolution of each product generation, n (SqeCl$_n$), shown in Fig. 1A appears statistical and is consistent with a sequential reaction model analysis[46] conducted by Popolan *et al.*[33] as well as other systems exhibiting multi-generational kinetics.[43–45] The sequential reaction model applies to particles that are well-mixed on the timescale of the reaction, where the population of reactive species in the aerosol (*i.e.* Sqe, SqeCl$_n$) is a Poisson distribution[46] (eqn (2)) that evolves with chlorine exposure ([Cl$_2$]t).

$$f(n, [Cl_2]t) = \frac{[SqeCl_{2n}]}{[Sqe]_0} = \frac{(k_{fit}[Cl_2]t)^n}{n!} e^{(-k_{fit}[Cl_2]t)} \quad (2)$$

[SqeCl$_{2n}$] is the concentration of product generation (n) and [Sqe]$_0$ is the initial Sqe concentration. k_{fit} is the second order heterogeneous rate constant, which is assumed, for simplicity, to be the same for all generations (*e.g.* Cl$_2$ + Sqe and Cl$_2$ + SqeCl$_n$). Eqn (2) can reasonably account for the kinetic evolution of the products (SqeCl$_2$, SqeCl$_4$ and SqeCl$_6$) as shown in Fig. 1A, which indicates that the chemical evolution of Sqe and SqeCl$_n$ can be well represented by the same rate constant k_{fit}, indicating that $\gamma_{eff}^{Sqe} \approx \gamma_{eff}^{SqeCl_2} \approx \gamma_{eff}^{SqeCl_4} \approx \gamma_{eff}^{SqeCl_6}$.

The temperature dependence of the Sqe + Cl$_2$ reaction is measured at 5, 25 and 50 °C. As shown in Fig. 2A, the Sqe reaction rate gets faster as the temperature is lowered (*e.g.* 50 to 5 °C). As expected, γ_{eff}^{Sqe} also increases with decreasing temperature as shown in Fig. 2B, with the reaction proceeding ~5× faster at 5 °C compared to 50 °C. Although the reaction rate increases with decreasing temperature, the product formation kinetics remain sequential (*i.e.* $\gamma_{eff}^{Sqe} \approx \gamma_{eff}^{SqeCl_2} \approx \gamma_{eff}^{SqeCl_4} \approx \gamma_{eff}^{SqeCl_6}$)
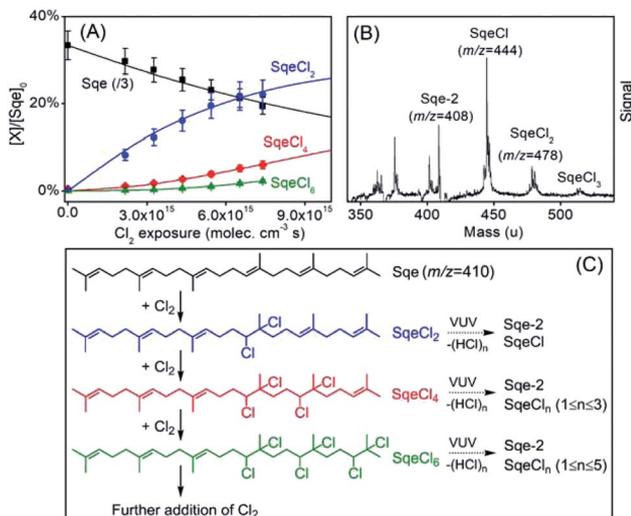

Fig. 1 (A) Normalized concentrations of Sqe and SqeCl$_n$ as a function of chlorine exposure ([Cl$_2$] × time). The normalized concentration of Sqe is divided by three (*i.e.* /3) for ease of presentation. Symbols are experiments. Solid lines are predictions by the sequential reaction model described in eqn (2). (B) Difference mass spectra (reacted–unreacted Sqe) showing the SqeCl$_n$ reaction products. (C) A reaction scheme showing the first three product generations (n), as well as the dissociative photoionization pathways that involve one or more –HCl eliminations.
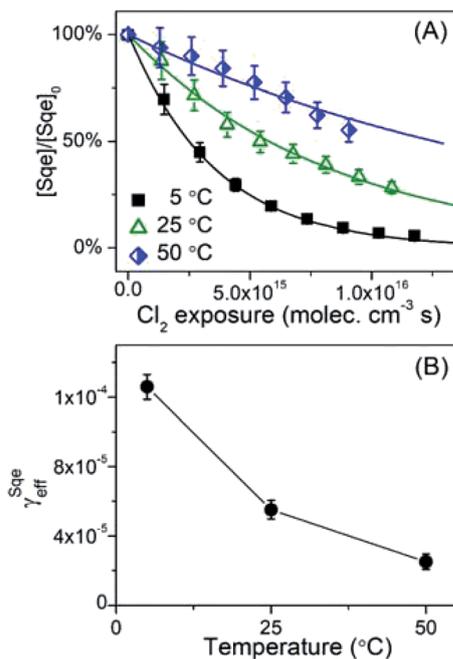
Fig. 2 (A) Normalized decay of Sqe as a function of Cl_2 exposure at 5, 25 and 50 °C. Symbols are experimental data; solid lines are predictions from the sequential reaction model. (B) γ_{eff}^{Sqe} as a function of temperature. Symbols are experimental data, which are connected by solid lines to guide the eye.

and the product mass spectra (Fig. 1B) are nearly identical for all temperatures. This suggests that the overall mechanism does not change with temperature, but rather just the overall rate of chlorination.

While this negative temperature dependence is somewhat unusual for chemical reactions occurring in single phase, it does occur for multistep reactions that proceed through a potential well or pre-reactive complex. Trace gas uptake at droplet surfaces often exhibit a negative temperature dependence, since mass accommodation is controlled by multiple elementary steps as shown in Fig. 3.[1-5,47-50] Without reaction, there are two coupled equilibria that control the concentration
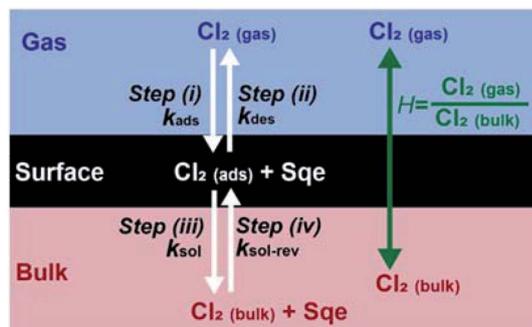

Fig. 3 Schematic of gas uptake at an aerosol surface showing adsorption, desorption, solvation, de-solvation steps (denoted as steps (i) to (iv)), as well as the chemical reactions. The net Henry's law constant (H) is also shown.

of Cl_2 in the aerosol. The first equilibrium describes the partitioning of gas phase $Cl_{2(gas)}$ to form an adsorbed species (i.e. $Cl_{2(ads)}$), whose steady state concentration is controlled by the rate constants for Cl_2 adsorption (k_{ads}) to and desorption (k_{des}) from the interface (steps (i) and (ii) in Fig. 3). The second equilibrium describes the partitioning of $Cl_{2(ads)}$ to the bulk ($Cl_{2(bulk)}$) and is governed by the solvation (k_{sol}) and de-solvation ($k_{sol-rev}$) rate constants shown in steps (iii) and (iv) in Fig. 3. The product of these two equilibria is the Henry's law constant (H) for Cl_2. Diffusion pathways are not explicitly shown in Fig. 3.

For the system considered here there are reaction steps in the bulk and at the surface. The reacto-diffusive length (L) of Cl_2 in Sqe is,

$$L = \sqrt{\frac{D}{k_{rxn}[Sqe]}} \tag{3}$$

where D is the diffusion coefficient of Cl_2 and k_{rxn} is the bimolecular rate constant for the chlorination reaction. L is estimated to be ∼300 nm ($D = 1.38 \times 10^{-5}$ cm^2 s^{-1},[51] $k_{rxn} = 1.0 \times 10^{-17}$ cm^3 molecules^{-1} s^{-1},[52] [Sqe] = 1.26×10^{21} molecules cm^{-3}), which is ∼2× larger than the average aerosol diameter used in the experiments. Additionally, Cl_2 is quite soluble in both hydrocarbons[53,54] (e.g. decane[55]) and in polymers[56,57] with a dimensionless Henry's law (H_{cc}) constant between 10–20. Thus chlorination is expected to occur within the volume of the particle. However, despite this expectation that chlorination occurs mainly in the bulk (as suggested by eqn (3)), the temperature dependence of the uptake coefficient, estimated using a resistor model explicitly neglecting surface processes, predicts that the uptake coefficient will actually decrease with temperature as shown in Fig. S1 and described in the ESI.† This is opposite of the experimental trend and suggests the importance of surface process in governing the observed uptake coefficient.[58]

As shown previously for many systems,[1-4,47-50] the negative temperature dependence observed for the mass accommodation coefficient arises from the aggregate temperature dependence of the individual surface steps shown in Fig. 3. The negative temperature dependence observed in Fig. 2B is likely of similar origin.[4,47,48] From previous studies,[59] the adsorption step k_{ads} is assumed to have no barrier and expected to be nearly temperature independent with only slight changes arising from the temperature dependence of the Cl_2 velocity. The negative dependence[48,60] is mainly controlled by surface desorption (k_{des}, step (ii), Fig. 3) and solvation (k_{sol}, step (iii), Fig. 3), however the exact scaling and magnitude of these individual rates is model dependent. From molecular beam scattering experiments, k_{des} is expected to decrease with temperature following an Arrhenius relationship: as temperature decreases, desorption time lengthens and k_{des} becomes smaller.[61] The temperature dependence of k_{sol} is more ambiguous in prior studies. In some studies,[59,60,62] k_{sol} is thought to be weakly temperature dependent, varying much more slowly than desorption due to the smaller activation energy for solvation. The critical cluster nucleation model[60] predicts an increase of k_{sol} with decreasing temperature, whereas the Gibb's surface model[60] predicts the

opposite – a slight decrease. In Molecular Dynamics (MD) simulations[63–65] there doesn't appear to be a substantial barrier for solvation, as predicted by the nucleation model. To our knowledge, there remains a substantial uncertainty in how to reconcile these various model predictions (MD, critical cluster nucleation,[49] capillary wave[66]) of trace gas uptake with experimental measurements,[1,2,60,67,68] which is needed to produce a self-consistent set of kinetic parameters that vary with temperature.

Despite this uncertainty, the temperature dependence shown in Fig. 2B can be reasonably interpreted as follows. Since the reacto-diffusive length is larger than the particle diameter, the chlorination reaction is expected to occur throughout the particle volume. So as temperature decreases so does k_{des}, leading to an increase in $[Cl_{2(ads)}]$, which will increase both the chlorination rate at the interface as well as the rate of solvation (*i.e.* $Cl_{2(ads)} \rightarrow Cl_{2(bulk)}$), which in turn increases the chlorination rate in the bulk. Effectively, a decrease in k_{des} (or k_{sol}) at low temperatures, increases the net Henry's law constant (H) for Cl_2, since it is product of the two equilibria shown in Fig. 3.

In order to further explore the origin of the accelerated heterogeneous reaction rates at low temperature, a series of isothermal experiments are conducted to examine how spectator molecules containing oxygenated functional groups modify the chlorination rate of Sqe in a similar way as decreasing the temperature.

(b) Accelerated rates in Sqe/alcohol mixtures

2-Decyl-1-tetradecanol ($C_{24}H_{50}O$, termed $C_{24}OH$) is mixed with Sqe to make an aerosol of binary composition. $C_{24}OH$ is saturated and thus unreactive towards Cl_2. As shown in Fig. 4A, the

decay of Sqe in the binary mixture is faster when compared to the reactivity of neat Sqe. Fig. 4B shows γ_{eff}^{Sqe} as a function of $C_{24}OH$ mole fraction, which is observed to steeply increase and then plateau at 8×10^{-4} when the aerosol is $\sim$12–15% $C_{24}OH$. γ_{eff}^{Sqe} in the mixture is 23 times larger than for the neat Sqe experiment (3.5×10^{-5}). As discussed below we find no evidence that the presence of $C_{24}OH$ alters the product composition.

The plateau shown in Fig. 4B suggests that $C_{24}OH$ partitions to the aerosol surface and tends towards saturation as its bulk mole fraction is increased. The steep increase and saturation of γ_{eff}^{Sqe} is different from the monotonic increase one would expect for the alternative case where the bulk solubility of Cl_2 is substantially larger in $C_{24}OH$ than in Sqe. Previous computational and experimental studies, on reasonably analogous systems, support these observations; namely that oxygenated solutes (*e.g.* $C_{24}OH$, ethanol, and other oxygenates) generally partition to the surface of a hydrocarbon solvent. For example, Pecsok and Gump[69] found that the surface tension of squalane (saturated analog of Sqe) decreases steeply when mixed with a small amount of ethanol. At ethanol mole fractions of $\sim$0.02, the squalane/ethanol solution exhibits a surface tension that is nearly identical to that of the pure ethanol liquid. A Molecular Dynamics study of squalane, reported by Wick *et al.*,[70] found that for 1-butanol the gas–surface partitioning coefficient was $\sim$1.5 $\times$ larger than the gas–bulk partitioning coefficient, indicating interfacial enrichment. Another study[71] of the partitioning of alkanols in squalane found that surface partitioning increased with alcohol carbon number, with the surface partitioning coefficient of 4-heptanol and 2-heptanol being 10 to 100 times larger than that of ethanol, respectively.[69]
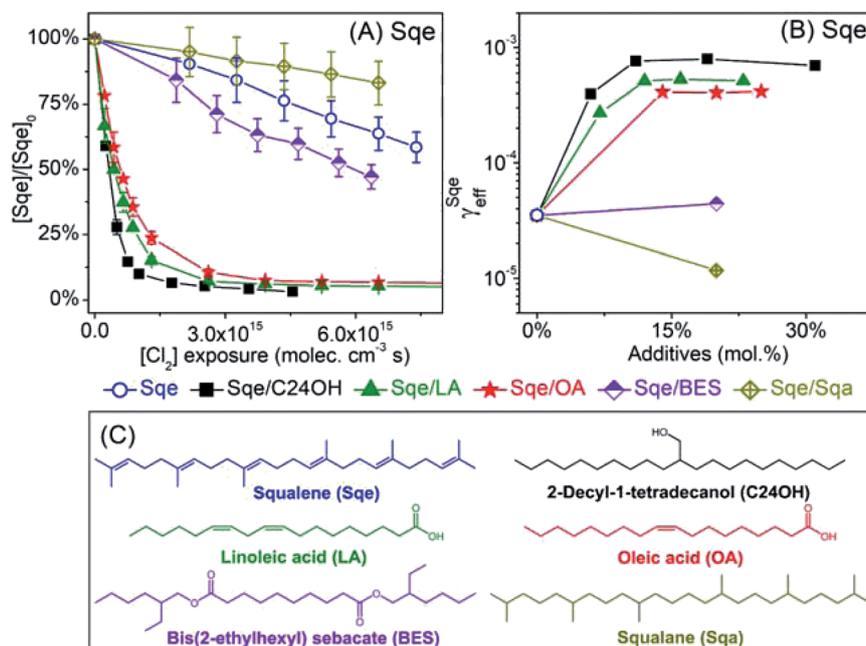

Fig. 4 (A) Normalized decay of Sqe as a function of Cl_2 exposure for neat Sqe and Sqe + additive (*i.e.* $C_{24}OH$, LA, OA, BES and Sqa) experiments. (B) γ_{eff}^{Sqe} as a function of additive mole fraction. Symbols are experimental data, which are connected by solid lines to guide the eye. (C) Chemical structures of Sqe and the liquid additives.
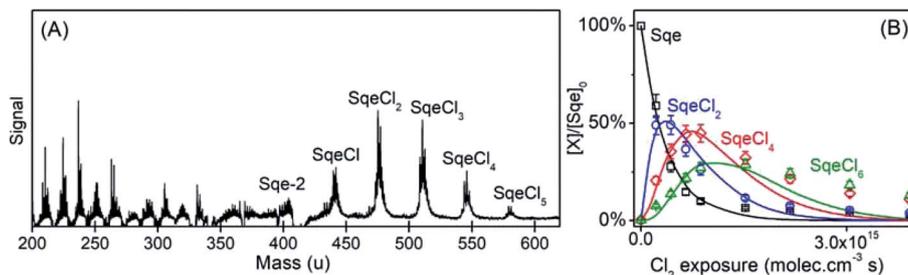
Fig. 5 (A) Difference mass spectra (reacted−unreacted Sqe) showing the reaction products ($SqeCl_n$); (B) Decay of Sqe and the formation kinetics of $SqeCl_n$ in the Sqe/$C_{24}OH$ mixture experiment. Symbols are experimental data; solid lines are generated from the sequential reaction model in eqn (2).

Fig. 5A shows the reaction products formed in the Sqe/$C_{24}OH$ mixture experiment. The major products are the same series of $SqeCl_n$ peaks that were observed in the neat Sqe reaction (Fig. 1). This is expected since $C_{24}OH$ lacks reactive sites for electrophilic addition of Cl_2. The kinetics, shown in Fig. 5B, although faster, remain sequential (i.e. $\gamma_{eff}^{Sqe} \approx \gamma_{eff}^{SqeCl_2} \approx \gamma_{eff}^{SqeCl_4} \approx \gamma_{eff}^{SqeCl_6}$) in the presence of $C_{24}OH$.

In summary, we find evidence for the surface partitioning of $C_{24}OH$, but no evidence that its presence in the aerosol forms new reaction products, which would suggest an altered reaction mechanism (e.g. chlorohydrin formation[39]). Rather, the alcohol appears only to accelerate the sequential addition of chlorine to Sqe without directly participating in the mechanism (i.e. a catalyst). Together these observations suggest that the acceleration mechanism involves a slowing of the Cl_2 desorption kinetics (in analogous way as decreasing temperature for the neat Sqe reaction) likely through the stronger binding of Cl_2 to the –OH moiety of $C_{24}OH$. This is consistent with the delayed desorption of gas when forming interfacial hydrogen-bonds, as reported by Morris and coworkers.[61] Thus, any decrease in k_{des}, due to halogen-bonding, will enhance both the chlorination rate of Sqe at the interface as well as solvation rate of $Cl_{2(ads)}$, which together would account for the accelerated kinetics.

Fig. 6A shows the temperature dependence of the Sqe decay kinetics in a binary mixture with $C_{24}OH$. Although the decay of Sqe in the mixture becomes more rapid as temperature is reduced to 5 °C, the temperature dependence of the uptake coefficient is much weaker in the mixture than the pure Sqe aerosol (Fig. 6B). An Arrhenius analysis of the temperature dependence in Fig. 6B yields a phenomenological activation energy of −26.7 kJ mol^{-1} for pure Sqe and −13.9 kJ mol^{-1} for the Sqe/$C_{24}OH$ mixture. In the past, the temperature dependence of the mass accommodation coefficient is used to extract information about the energetic barriers for non-reactive and in some cases reactive uptake. However, the interpretation of the energies extracted from the data in Fig. 6B in terms of simple energetic barriers is more ambiguous due to the complex coupling of the equilibria and surface/bulk reaction pathways shown in Fig. 3.

(c) Accelerated rates in Sqe/fatty acid mixtures

Aerosols containing binary mixtures of Sqe and two liquid fatty acids are used to further evaluate the role of oxygenated

functional groups (i.e. –COOH) in accelerating the chlorination of squalene. Unlike $C_{24}OH$, linoleic acid (LA) and oleic acid (OA) have C=C bond(s), and react with Cl_2. LA and OA reside together with Sqe in skin lipids.[34] Fig. 4A shows the decay of Sqe in binary mixtures with either LA or OA. The presence of these fatty acids leads to faster decay kinetics for Sqe than for the neat case. As observed with $C_{24}OH$, there is a steep increase of γ_{eff}^{Sqe} with LA and OA mole fraction, reaching a plateau of $\gamma_{eff}^{Sqe} = 5.3 \times 10^{-4}$ and 4.17×10^{-4}, which is around 16 and 12 times faster than the reaction rate of pure Sqe.

Fig. 7 compares the products formed in the Sqe/LA (or OA) mixture with results obtained using pure LA (or OA). In addition to the series of products originating from Sqe (i.e. $SqeCl_n$), there
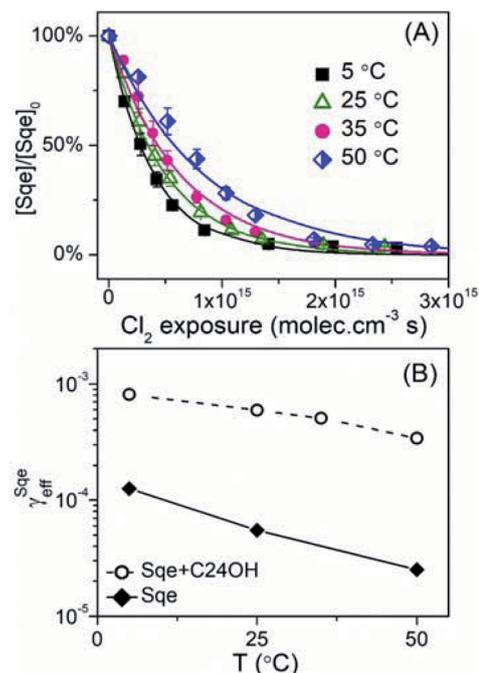

Fig. 6 (A) Normalized decay of Sqe as a function of Cl_2 exposure for Sqe/$C_{24}OH$ as a function of temperature (5, 25, 35 and 50 °C). Symbols are experimental data; solid lines are from the sequential reaction model. (B) γ_{eff}^{Sqe} as a function of temperature for pure Sqe (solid symbols), and the Sqe/$C_{24}OH$ mixture experiments (open symbols). Symbols are experimental data, which are connected by lines to guide the eye.

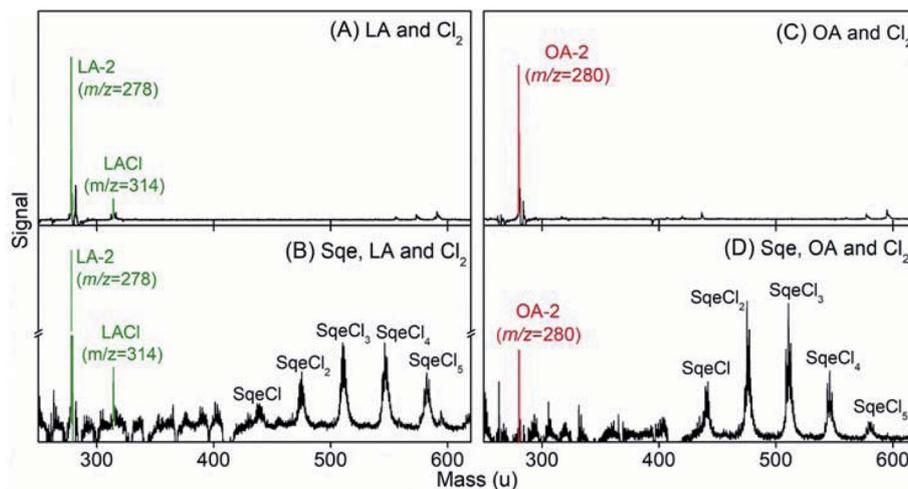Fig. 7 Difference mass spectra showing reaction products (SqeCl$_n$, LACl$_n$ and OACl$_n$) during the heterogeneous reaction of Cl$_2$ in (A) neat LA; (B) the Sqe/LA mixture; (C) neat OA; and (D) the Sqe/OA mixture experiments, respectively.

appears new species that arise from the reaction of Cl$_2$ with OA and LA. This is expected since the C=C bond(s) in LA and OA react with Cl$_2$ to produce LACl$_n$ (detected as LA-2 and LACl) and OACl$_n$ (detected as OA-2) products as shown in Fig. 7. These LACl$_n$ and OACl$_n$ products are the same as those in pure aerosols of LA (or OA) as shown in Fig. 7A and C. The reaction pathways for the formation of these chlorinated products and the mass spectral peak patterns, after accounting for –(HCl)$_n$ elimination, are shown in Fig. S2 and S3 in the ESI.† These patterns are consistent with the dissociative photoionization pathways observed for SqeCl$_n$ and described above.

Besides SqeCl$_n$, LACl$_n$ and OACl$_n$, no new products, beyond what is observed for pure LA and OA, are detected in the mixed aerosols, which suggest that the presence of these fatty acids does not alter the reaction pathway of Sqe itself. This is consistent with Sqe/C$_{24}$OH experiment described above. Additional experimental evidence and checks for Sqe/LA system can be found in Fig. S4 and S5 in the ESI.†

It is interesting to note that the acceleration of the Sqe kinetics in the presence of LA (or OA) is only slightly smaller than that observed for C$_{24}$OH as shown in Fig. 4B. This suggests that the key moiety that enhances the kinetics is the –OH rather than the –C=O group.

(d) Accelerated and decelerated heterogeneous rates of Sqe in the presence of BES and Sqa

To examine the role of the –C=O group on the rate acceleration, a liquid ester, bis(2-ethylhexyl) sebacate (BES), is mixed with Sqe as shown in Fig. 4C. BES has a saturated carbon backbone, which is unreactive towards Cl$_2$. As shown in Fig. 4, the presence of BES slightly accelerates the decay of Sqe, with a $\gamma_{\text{eff}}^{\text{Sqe}}$ that is only 26% larger than is observed for the pure Sqe case. This indicates, assuming that interfacial orientation plays a minor role, that the –C=O portion of BES only slightly increases the reaction rate, suggesting that the largest contribution to reaction acceleration is from the –OH group in the acids. For a final

comparison, a saturated alkane, squalane (Sqa), is added to Sqe. Sqa has a similar branched structure as Sqe, but lacks C=C bonds as shown in Fig. 4C. In this binary mixture, $\gamma_{\text{eff}}^{\text{Sqe}}$ decreases by 66% relative to pure Sqe.

As shown above for the Sqe/C$_{24}$OH experiment, the same set of Sqe reaction products are observed to form sequentially in the LA, OA, BES and Sqa mixtures, albeit their formation kinetics are either accelerated or decelerated when compared to the pure Sqe aerosol. This is illustrated in Fig. 8A where the formation and subsequent consumption kinetics of SqeCl is observed to be most rapid for the Sqe/C$_{24}$OH mixture, followed by Sqe/LA, Sqe/OA, Sqe/BES, pure Sqe and Sqe/Sqa, respectively. The product formation kinetics mirror the trend in $\gamma_{\text{eff}}^{\text{Sqe}}$ observed in Fig. 4A. This is illustrated in Fig. 8B where the kinetics are recast in terms of Sqe lifetimes (τ_{Sqe}) instead of Cl$_2$ exposure as shown in Fig. 8A. τ_{Sqe} is the product of Cl$_2$ exposure (molecules per cm^3 × s) and the inverse Sqe decay constant, 1/k_{fit}. Fig. 8B shows that the evolution of SqeCl in pure Sqe aerosol and in the various binary mixtures as a function of τ_{Sqe} are identical within error. This indicates that the presence of the aerosol additives doesn't change the overall reaction mechanism but rather these additives serve only to modulate the overall rate of sequential addition of Cl$_2$ to Sqe and its chlorination products.

To summarize, the reactivity of Sqe can vary by over an order of magnitude and depends upon temperature and molecules co-present with Sqe in the aerosol. We find no evidence that these additives (or temperature) alter the Sqe + Cl$_2$ mechanism through the formation of new products or by deviations from the sequential reaction mechanism. Instead, we find that the magnitude of $\gamma_{\text{eff}}^{\text{Sqe}}$ scales with the molecular structure of the additive, with clear evidence that oxygenated functional groups accelerate the heterogeneous chlorination of Sqe. The observed order of decreasing heterogeneous reactivity by functional group is: –OH > –COOH > –C=O > C=C > C–C. This pattern appears consistent with the expected interaction strength of Cl$_2$ with various functional groups, pointing to the importance of
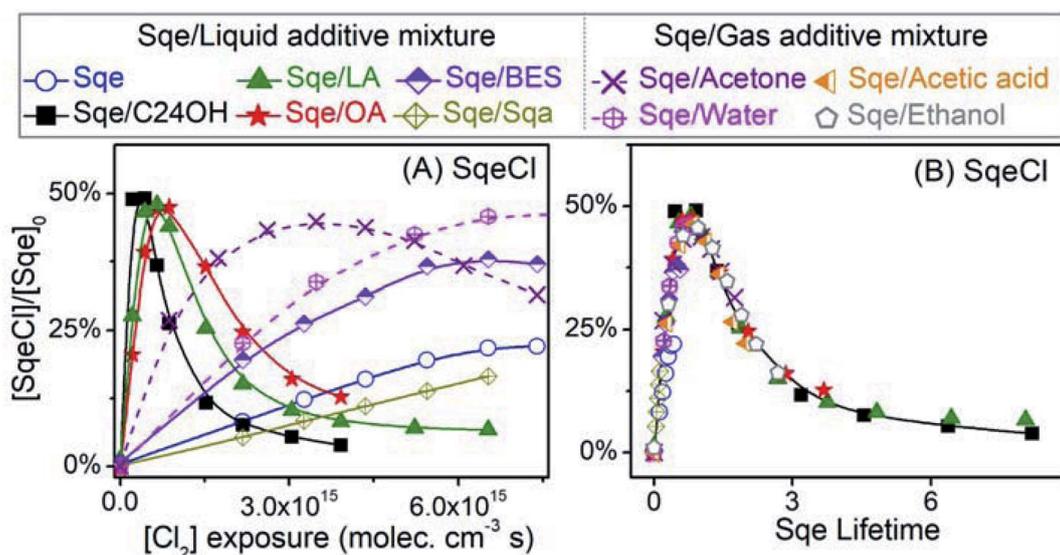
Fig. 8 Formation kinetics of SqeCl in pure Sqe aerosols, Sqe/C$_{24}$OH, Sqe/LA, Sqe/OA, Sqe/BES and Sqe/Sqa aerosol mixtures, and Sqe aerosols with gas additives (*i.e.* acetone, water, acetic acid, ethanol): (A) as a function of Cl$_2$ exposure; or (B) as a function of Sqe lifetime (τ_{Sqe}). Symbols are experimental data, which are connected by lines to guide the eye.

halogen bonding in promoting heterogeneous reactivity in the system. For example, from calculations it is observed that the interaction of Cl$_2$ with –OH groups is more favorable than with C=C bonds.[30] It seems likely that the additives (as well as reducing temperature) prolong the lifetime of Cl$_2$ at the aerosol surface, allowing increased flux through those pathways that culminate in a reaction, either directly at the interface or *via* reaction in the bulk after solvation of Cl$_{2(ads)}$. This conclusion will be further tested by introducing small oxygenated spectator molecules, as additives to the gas phase.

(e) Heterogeneous chlorination of Sqe with gas phase additives

Gas phase additives are introduced to the reactor by passing N$_2$ through a glass bubbler filled with either water, ethanol, acetic

acid, or acetone. The vapor concentration is controlled by changing the fraction of the total N$_2$ flow that is diverted through the bubbler. Fig. 9A shows that Sqe decays faster with increasing water vapor concentration ([H$_2$O]). γ_{eff}^{Sqe} increases monotonically with [H$_2$O], reaching a value at [H$_2$O] = 4.2 × 10^{17} molecues cm^{-3}, that is 45% faster than under dry conditions (Fig. 9C). These observations are consistent with a recent study that has confirmed the presence of adsorbed water at the squalene/air interface.[72]

Sqe decays more rapidly (up to 10×) with increasing concentrations of ethanol vapor as shown in Fig. 9B. This is also observed for acetic acid and acetone vapor. These results are summarized in Fig. 9C where γ_{eff}^{Sqe} shows a monotonic increase with additive concentration over what is observed for Sqe in the presence of N$_2$ only. In each case γ_{eff}^{Sqe} does not reach a plateau as was observed for the longer chain alcohol and fatty acid
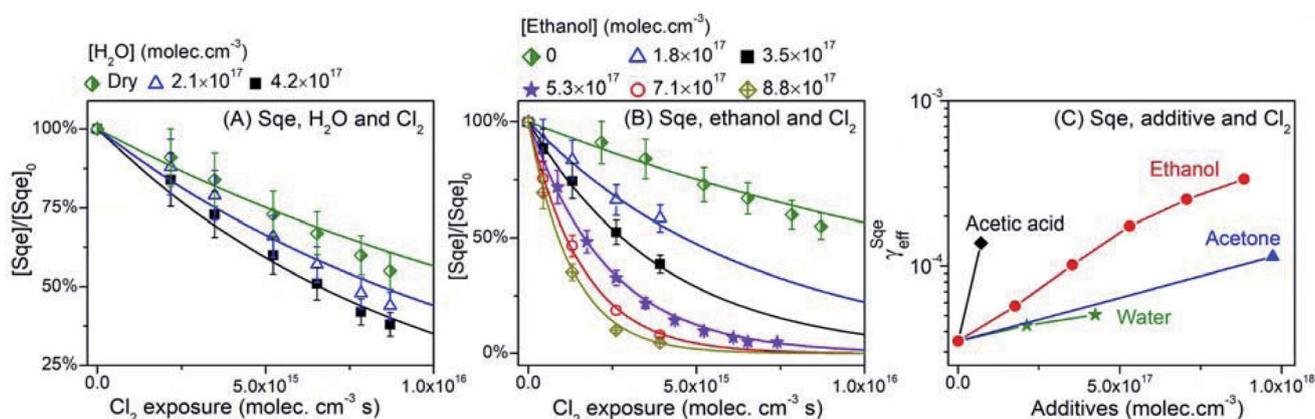

Fig. 9 Normalized decay of Sqe as a function of Cl$_2$ exposure and gas phase additives concentration: (A) H$_2$O and (B) ethanol. (C) γ_{eff}^{Sqe} as a function of gas phase additive concentration.

aerosol mixtures shown in Fig. 4B. This likely means, for example, that ethanol does not reach high enough concentrations in our reactor to saturate the aerosol surface. The order of reaction acceleration normalized to gas phase concentration is: acetic acid > ethanol > acetone $\geq$ water. Direct comparison with the aerosol additive trend in Fig. 4 is somewhat difficult, since the magnitude of reaction acceleration will depend both upon the strength of halogen bonding to Cl_2 as well as the partitioning of these small molecules to the aerosol surface, which will roughly scale with their relative vapor pressure.

The first generation reaction product (*i.e.* SqeCl) produced in the presence of these small gas phase molecules is plotted *versus* chlorine exposure and Sqe lifetime in Fig. 8. When normalized to Sqe lifetime the product formation kinetics are nearly identical to the binary mixture results. This suggests that in addition to aerosol phase additives, small gas phase molecules co-adsorbed to the aerosol surface can prolong the lifetime of Cl_2 providing additional time for the chlorination reaction to occur. These results appear consistent with previous studies of the enhanced uptake of HCl gas onto organic liquids in the presence of co-adsorbed H_2O, which is facilitated by the formation of H_2O–HCl complexes as reported in the ref. 73.

Conclusions

Experimental evidence is presented that both gas and aerosol phase molecules, which have oxygenated functional groups, catalyze the heterogeneous chlorination of an alkene leading to, in some cases, a 20× enhancement in the reaction rate. This behavior is similar to reducing temperature, which is known to slow the desorption kinetics relative to competing elementary steps that ultimately lead to solvation and reaction. For certain additives (ester and alkane), the heterogeneous reaction rate of Cl_2 with Sqe remains unchanged or is even slightly decelerated, which suggest weaker halogen bonding and larger values for k_{des} for these systems. We find no evidence that either the gas or aerosol phase additives modify the reaction mechanism.

Instead, these additives behave as spectators that either accelerate or decelerate the sequential formation of chlorinated Sqe reaction products. Together these results all point to the significant role that halogen bonding might play in this heterogeneous reaction. We propose that the formation of these relatively weak directional interactions between the oxygenated functional groups and Cl_2 slows its desorption rate (*i.e.* a smaller k_{des}) from the aerosol surface, thereby enhancing those pathways (solvation and reaction) that increase the rate of electrophilic addition. A full kinetic analysis of this data set will be conducted in a forthcoming publication to examine quantitatively the coupling of reaction, adsorption, solvation, desolvation, and reaction rates on the observed reactive uptake kinetics.

Finally, it is likely, and has indeed been shown theoretically that weak interactions, such as halogen and hydrogen bonding at aerosol surfaces can play a substantial role in determining heterogeneous reaction rates and mechanisms.[8–11] The chlorination reaction studied here is perhaps unique in that it is relatively slow reaction compared to others (*e.g.* ozonolysis and free radical reactions), thereby allowing the coupling and competition of the elementary steps shown in Fig. 3 to be more easily observed.

It is also interesting to consider the implication of these results for indoor surface chemistry.[23,24,38] Sqe, LA and OA are all important constituents of skin lipids, which act as a natural defense against the reactive oxygen and chlorine species. The half-life ($\tau_{1/2}$) of Sqe (in the absence of additives) is ~56 min under indoor conditions when bleach is used ([Cl_2] ~ 100 ppb).[35,37] However, in a mixture with other skin lipids such as LA (or OA), $\tau_{1/2}$ for Sqe decreases substantially to ~3.6 min at the same [Cl_2]. This indicates that skin lipid reactivity is a more complex function of the surface and gas phase environment, in which trace constituents and weak interactions play more important roles that previously imagined.

Data availability

The authors confirm that the data supporting the findings of this work are available within the article and its ESI.

Author contributions

M. Z. and K. R. W. designed the experiment. M. Z. made the experimental measurements and conducted the analysis of the data. M. Z. and K. R. W. wrote the manuscript.

Conflicts of interest

The authors declare no competing financial interest.

Acknowledgements

References

1 P. Davidovits, C. E. Kolb, L. R. Williams, J. T. Jayne and D. R. Worsnop, Mass accommodation and chemical reactions at gas-liquid interfaces, *Chem. Rev.*, 2006, **106**, 1323–1354.

2 P. Davidovits, C. E. Kolb, L. R. Williams, J. T. Jayne and D. R. Worsnop, Update 1 of: Mass accommodation and chemical reactions at gas-liquid interfaces, *Chem. Rev.*, 2011, **111**, PR76–PR109.

3 G. M. Nathanson, Molecular beam studies of gas-liquid interfaces, *Annu. Rev. Phys. Chem.*, 2004, **55**, 231–255.

4 G. M. Nathanson, P. Davidovits, D. R. Worsnop and C. E. Kolb, Dynamics and kinetics at the gas-liquid interface, J. Phys. Chem., 1996, 100, 13007–13020.

5 M. Galib and D. T. Limmer, Reactive uptake of N_2O_5 by atmospheric aerosol is dominated by interfacial processes, Science, 2021, 371, 921–925.

6 T. Moise and Y. Rudich, Uptake of Cl and Br by organic surfaces – a perspective on organic aerosols processing by tropospheric oxidants, Geophys. Res. Lett., 2001, 28, 4083–4086.

7 G. Rovelli, M. I. Jacobs, M. D. Willis, R. J. Rapf, A. M. Prophet and K. R. Wilson, A critical analysis of electrospray techniques for the determination of accelerated rates and mechanisms of chemical reactions in droplets, Chem. Sci., 2020, 11, 13026–13043.

8 R. D. Hoehn, M. A. Carignano, S. Kais, C. Zhu, J. Zhong, X. C. Zeng, J. S. Francisco and I. Gladich, Hydrogen bonding and orientation effects on the accommodation of methylamine at the air-water interface, J. Chem. Phys., 2016, 144, 214701.

9 M. Kumar and J. S. Francisco, Reactions of Criegee Intermediates with Non-Water Greenhouse Gases: Implications for Metal Free Chemical Fixation of Carbon Dioxide, J. Phys. Chem. Lett., 2017, 8, 4206–4213.

10 M. Kumar, J. Zhong, X. C. Zeng and J. S. Francisco, Reaction of Criegee intermediate with nitric acid at the air-water interface, J. Am. Chem. Soc., 2018, 140, 4913–4921.

11 M. Kumar, T. Trabelsi, J. C. Gomez Martin, A. Saiz-Lopez and J. S. Francisco, HIO_x-$IONO_2$ dynamics at the air-water interface: revealing the existence of a halogen bond at the atmospheric aerosol surface, J. Am. Chem. Soc., 2020, 142, 12467–12477.

12 E. M. Knipping, M. J. Lakin, K. L. Foster, P. Jungwirth, D. J. Tobias, R. B. Gerber, D. Dabdub and B. J. Finlayson-Pitts, Experiments and simulations of ion-enhanced interfacial chemistry on aqueous NaCl aerosols, Science, 2000, 288, 301–306.

13 M. Jang, N. M. Czoschke, S. Lee and R. M. Kamens, Heterogeneous atmospheric aerosol production by acid-catalyzed particle-phase reactions, Science, 2002, 298, 814–817.

14 B. J. Finlayson-Pitts and J. N. Pitts Jr, Tropospheric air pollution: ozone, airborne toxics, polycyclic aromatic hydrocarbons, and particles, Science, 1997, 276, 1045–1051.

15 A. Mellouki, T. J. Wallington and J. Chen, Atmospheric chemistry of oxygenated volatile organic compounds: impacts on air quality and climate, Chem. Rev., 2015, 115, 3984–4014.

16 R. J. Charlson, S. E. Schwartz, J. M. Hales, R. D. Cess, J. J. A. Coakley, J. E. Hansen and D. J. Hofmann, Climate forcing by anthropogenic aerosols, Science, 1992, 255, 423–430.

17 V. Ramanathan, P. J. Crutzen, J. T. Kiehl and D. Rosenfeld, Aerosols, climate, and the hydrological cycle, Science, 2001, 294, 2119–2124.

18 M. Kanakidou, J. H. Seinfeld, S. N. Pandis, I. Barnes, F. J. Dentener, M. C. Facchini, R. V. Dingenen, B. Ervens, A. Nenes, C. J. Nielsen, E. Swietlicki, J. P. Putaud, Y. Balkanski, S. Fuzzi, J. Horth, G. K. Moortgat, R. Winterhalter, C. E. L. Myhre, K. Tsigaridis, E. Vignati, E. G. Stephanou and J. Wilson, Organic aerosol and global climate modelling: a review, Atmos. Chem. Phys., 2005, 5, 1053–1123.

19 U. Poschl, Atmospheric aerosols: composition, transformation, climate and health effects, Angew. Chem., Int. Ed., 2005, 44, 7520–7540.

20 J. B. Burkholder, J. P. D. Abbatt, I. Barnes, J. M. Roberts, M. L. Melamed, M. Ammann, A. K. Bertram, C. D. Cappa, A. G. Carlton, L. J. Carpenter, J. N. Crowley, Y. Dubowski, C. George, D. E. Heard, H. Herrmann, F. N. Keutsch, J. H. Kroll, V. F. McNeill, N. L. Ng, S. A. Nizkorodov, J. J. Orlando, C. J. Percival, B. Picquet-Varrault, Y. Rudich, P. W. Seakins, J. D. Surratt, H. Tanimoto, J. A. Thornton, Z. Tong, G. S. Tyndall, A. Wahner, C. J. Weschler, K. R. Wilson and P. J. Ziemann, The Essential Role for Laboratory Studies in Atmospheric Chemistry, Environ. Sci. Technol., 2017, 51, 2519–2528.

21 Y. Liu, A. G. Bé, V. W. Or, M. R. Alves, V. H. Grassian and F. M. Geiger, Challenges and Opportunities in Molecular-Level Indoor Surface Chemistry and Physics, Cell Rep. Phys. Sci., 2020, 1, 100256.

22 C. J. Weschler and N. Carslaw, Indoor Chemistry, Environ. Sci. Technol., 2018, 52, 2419–2428.

23 J. P. D. Abbatt and C. Wang, The atmospheric chemistry of indoor environments, Environ. Sci.: Processes Impacts, 2020, 22, 25–48.

24 A. P. Ault, V. H. Grassian, N. Carslaw, D. B. Collins, H. Destaillats, D. J. Donaldson, D. K. Farmer, J. L. Jimenez, V. F. McNeill, G. C. Morrison, R. E. O'Brien, M. Shiraiwa, M. E. Vance, J. R. Wells and W. Xiong, Indoor Surface Chemistry: Developing a Molecular Picture of Reactions on Indoor Interfaces, Chem, 2020, 6, 3203–3218.

25 S. Gligorovski and J. P. D. Abbatt, An indoor chemical cocktail, Science, 2018, 359, 632–633.

26 P. A. J. Bagot, C. Waring, M. L. Costen and K. G. McKendrick, Dynamics of Inelastic Scattering of OH Radicals from Reactive and Inert Liquid Surfaces, J. Phys. Chem. C, 2008, 112, 10868–10877.

27 M. F. Ruiz-Lopez, J. S. Francisco, M. T. C. Martins-Costa and J. M. Anglada, Molecular reactions at aqueous interfaces, Nat. Rev. Chem., 2020, 4, 459–475.

28 P. Metrangolo and G. Resnati, Halogen Versus Hydrogen, Science, 2008, 321, 918–919.

29 G. Cavallo, P. Metrangolo, R. Milani, T. Pilati, A. Priimagi, G. Resnati and G. Terraneo, The Halogen Bond, Chem. Rev., 2016, 116, 2478–2601.

30 S. J. Ang, A. M. Mak and M. W. Wong, Nature of halogen bonding involving pi-systems, nitroxide radicals and carbenes: a highlight of the importance of charge transfer, Phys. Chem. Chem. Phys., 2018, 20, 26463–26478.

31 M. E. Wolf, B. Zhang, J. M. Turney and H. F. Schaefer, A comparison between hydrogen and halogen bonding: the hypohalous acid–water dimers, HOX···H_2O (X = F, Cl, Br), Phys. Chem. Chem. Phys., 2019, 21, 6160–6170.

32 P. Auffinger, F. A. Hays, E. Westhof and P. S. Ho, Halogen bonds in biological molecules, *Proc. Natl. Acad. Sci. U. S. A.*, 2004, **101**, 16789–16794.

33 D. M. Popolan-Vaida, C.-L. Liu, T. Nah, K. R. Wilson and S. R. Leone, Reaction of chlorine molecules with unsaturated submicron organic particles, *Z. Phys. Chem.*, 2015, **229**, 1521–1540.

34 N. Nicolaides, Skin Lipids: Their Biochemical Uniqueness, *Science*, 1974, **186**, 19–26.

35 C. Wang, D. B. Collins and J. P. D. Abbatt, Indoor illumination of terpenes and bleach emissions leads to particle formation and growth, *Environ. Sci. Technol.*, 2019, **53**, 11792–11800.

36 J. P. S. Wong, N. Carslaw, R. Zhao, S. Zhou and J. P. D. Abbatt, Observations and impacts of bleach washing on indoor chlorine chemistry, *Indoor Air*, 2017, **27**, 1082–1090.

37 J. M. Mattila, C. Arata, C. Wang, E. F. Katz, A. Abeleira, Y. Zhou, S. Zhou, A. H. Goldstein, J. P. D. Abbatt, P. F. DeCarlo and D. K. Farmer, Dark Chemistry during Bleach Cleaning Enhances Oxidation of Organics and Secondary Organic Aerosol Production Indoors, *Environ. Sci. Technol. Lett.*, 2020, **7**, 795–801.

38 J. M. Mattila, P. S. J. Lakey, M. Shiraiwa, C. Wang, J. P. D. Abbatt, C. Arata, A. H. Goldstein, L. Ampollini, E. F. Katz, P. F. DeCarlo, S. Zhou, T. F. Kahan, F. J. Cardoso-Saldana, L. H. Ruiz, A. Abeleira, E. K. Boedicker, M. E. Vance and D. K. Farmer, Multiphase chemistry controls inorganic chlorinated and nitrogenated compounds in indoor air during bleach cleaning, *Environ. Sci. Technol.*, 2020, **54**, 1730–1739.

39 H. Schwartz-Narbonne, C. Wang, S. Zhou, J. P. D. Abbatt and J. Faust, Heterogeneous Chlorination of Squalene and Oleic Acid, *Environ. Sci. Technol.*, 2019, **53**, 1217–1224.

40 C. R. Ruehl, T. Nah, G. Isaacman, D. R. Worton, A. W. H. Chan, K. R. Kolesar, C. D. Cappa, A. H. Goldstein and K. R. Wilson, The Influence of Molecular Structure and Aerosol Phase on the Heterogeneous Oxidation of Normal and Branched Alkanes by OH, *J. Phys. Chem. A*, 2013, **117**, 3990–4000.

41 E. Gloaguen, E. R. Mysak, S. R. Leone, M. Ahmed and K. R. Wilson, Investigating the chemical composition of mixed organic–inorganic particles by "soft" vacuum ultraviolet photoionization: The reaction of ozone with anthracene on sodium chloride particles, *Int. J. Mass Spectrom.*, 2006, **258**, 74–85.

42 K. R. Wilson, M. Jimenez-Cruz, C. Nicolas, L. Belau, S. R. Leone and M. Ahmed, Thermal vaporization of biological nanoparticles: fragment-free vacuum ultraviolet photoionization mass spectra of tryptophan, phenylalanine-glycine-glycine, and β-carotene, *J. Phys. Chem. A*, 2006, **110**, 2106–2113.

43 J. D. Smith, J. H. Kroll, C. D. Cappa, D. L. Che, C. L. Liu, M. Ahmed, S. R. Leone, D. R. Worsnop and K. R. Wilson, The heterogeneous reaction of hydroxyl radicals with sub-micron squalane particles: a model system for understanding the oxidative aging of ambient aerosols, *Atmos. Chem. Phys.*, 2009, **9**, 3209–3222.

44 C. L. Liu, J. D. Smith, D. L. Che, M. Ahmed, S. R. Leone and K. R. Wilson, The direct observation of secondary radical chain chemistry in the heterogeneous reaction of chlorine atoms with submicron squalane droplets, *Phys. Chem. Chem. Phys.*, 2011, **13**, 8993–9007.

45 D. M. Popolan-Vaida, K. R. Wilson and S. R. Leone, Reaction of iodine atoms with submicrometer squalane and squalene droplets: mechanistic insights into heterogeneous reactions, *J. Phys. Chem. A*, 2014, **118**, 10688–10698.

46 K. R. Wilson, J. D. Smith, S. H. Kessler and J. H. Kroll, The statistical evolution of multiple generations of oxidation products in the photochemical aging of chemically reduced organic aerosol, *Phys. Chem. Chem. Phys.*, 2012, **14**, 1468–1479.

47 D. R. Worsnop, M. S. Zahniser, C. E. Kolb, J. A. Gardner, L. R. Watson, J. M. Van Doren, J. T. Jayne and P. Davidovits, Temperature dependence of mass accommodation of SO_2 and H_2O_2 on aqueous surfaces, *J. Phys. Chem.*, 1989, **93**, 1159–1172.

48 Q. Shi, P. Davidovits, J. T. Jayne, D. R. Worsnop and C. E. Kolb, Uptake of Gas-Phase Ammonia. 1. Uptake by Aqueous Surfaces as a Function of pH, *J. Phys. Chem. A*, 1999, **103**, 8812–8823.

49 P. Davidovits, J. T. Jayne, S. X. Duan, D. R. Worsnop, M. S. Zahniser and C. E. Kolb, Uptake of gas molecules by liquids: a model, *J. Phys. Chem.*, 1991, **95**, 6337–6340.

50 P. Davidovits, J. H. Hu, D. R. Worsnop, M. S. Zahniser and C. E. Kolb, Entry of gas molecules into liquids, *Faraday Discuss.*, 1995, **100**, 65–82.

51 A. Tang and O. C. Sandall, Diffusion Coefficient of Chlorine in Water at 25–60 °C, *J. Chem. Eng. Data*, 1985, **30**, 189–191.

52 K. Yates and H. W. Leung, Kinetics and Stereochemistry of the Addition of Chlorine to Styrenes, *J. Org. Chem.*, 1980, **45**, 1401–1406.

53 N. W. Taylor and J. H. Hildebrand, Solubility. VIII. Solubility Relations of Certain Gases, *J. Am. Chem. Soc.*, 1923, **45**, 682–694.

54 M. Lohse and W. D. Deckwer, Solubility of chlorine in benzene, toluene, ethylbenzene, *o*-, *m*-, and *p*-xylenes, and 2-, 3-, and 4-chlorotoluenes, *J. Chem. Eng. Data*, 1981, **26**, 159–161.

55 *IUPAC Solubility Data Series*, ed. C. L. Young, Pergamon Press, Oxford, England, 1983, ch. Sulfur Dioxide, Chlorine, Fluorine and Chlorine Oxides, vol. 12, p. 494.

56 S. Wachi, H. Morikawa and H. Inoue, Conversion distribution in diffusion-governed chlorination of poly(vinyl chloride), *AIChE J.*, 1988, **34**, 1683–1690.

57 R. Paterson, Y. Yampol'skii, P. G. T. Fogg, A. Bokarev, V. Bondar, O. Ilinich and S. Shishatskii, IUPAC-NIST Solubility Data Series 70. Solubility of Gases in Glassy Polymers, *J. Phys. Chem. Ref. Data*, 1999, **28**, 1255–1450.

58 L. Lee and K. Wilson, The Reactive-Diffusive Length of OH and Ozone in Model Organic Aerosols, *J. Phys. Chem. A*, 2016, **120**, 6800–6812.

59 L. Chaix, H. v. d. Bergh and M. J. Rossi, Real-Time Kinetic Measurements of the Condensation and Evaporation of D_2O Molecules on Ice at 140 K < T < 220 K, *J. Phys. Chem. A*, 1998, **102**, 10300–10309.

60 Q. Shi, Y. Q. Li, P. Davidovits, J. T. Jayne, D. R. Worsnop, M. Mozurkewich and C. E. Kolb, Isotope exchange for gas-phase acetic acid and ethanol at aqueous interfaces: a study of surface reactions, *J. Phys. Chem. B*, 1999, **103**, 2417–2430.

61 J. R. Lohr, B. S. Day and J. R. Morris, Scattering, accommodation, and trapping of HCl in collisions with a hydroxylated self-assembled monolayer, *J. Phys. Chem. B*, 2005, **109**, 15469–15475.

62 B. Fluckiger and M. J. Rossi, Common Precursor Mechanism for the Heterogeneous Reaction of D_2O, HCl, HBr, and HOBr with Water Ice in the Range 170–230 K: Mass Accommodation Coefficients on Ice, *J. Phys. Chem. A*, 2003, **107**, 4103–4115.

63 A. Morita and B. C. Garrett, Molecular theory of mass transfer kinetics and dynamics at gas–water interface, *Fluid Dyn. Res.*, 2008, **40**, 459–473.

64 M. A. Wilson and A. Pohorille, Adsorption and Solvation of Ethanol at the Water Liquid-Vapor Interface: A Molecular Dynamics Study, *J. Phys. Chem. B*, 1997, **101**, 3130–3135.

65 R. S. Taylor and B. C. Garrett, Accommodation of Alcohols by the Liquid/Vapor Interface of Water: Molecular Dynamics Study, *J. Phys. Chem. B*, 1999, **103**, 844–851.

66 C. J. H. Knox and L. F. Phillips, Capillary-Wave Model of Gas-Liquid Exchange, *J. Phys. Chem. B*, 1998, **102**, 8469–8472.

67 B. C. Garrett, G. K. Schenter and A. Morita, Molecular Simulations of the Transport of Molecules across the Liquid/Vapor Interface of Water, *Chem. Rev.*, 2006, **106**, 1355–1374.

68 P. Davidovits, D. R. Worsnop, L. R. Williams, C. E. Kolb and M. Gershenzon, Comment on "Mass Accommodation Coefficient of Water: Molecular Dynamics Simulation and Revised Analysis of Droplet Train/Flow Reactor Experiment", *J. Phys. Chem. B*, 2005, **109**, 14742–14746.

69 R. L. Pecsok and B. H. Gump, Gas-liquid interface and solid support effects of polar solute-nonpolar solvent systems in gas chromatography, *J. Phys. Chem.*, 1967, **71**, 2202–2209.

70 C. D. Wick, J. I. Siepmann and M. R. Schure, Molecular Simulation of Concurrent Gas–Liquid Interfacial Adsorption and Partitioning in Gas–Liquid Chromatography, *Anal. Chem.*, 2002, **74**, 3518–3524.

71 M. Tascon, L. M. Romero, A. Acquaviva, S. Keunchkarian and C. Castells, Determinations of gas–liquid partition coefficients using capillary chromatographic columns. Alkanols in squalane, *J. Chromatogr. A*, 2013, **1294**, 130–136.

72 M. von Domaros, Y. Liu, J. L. Butman, E. Perlt, F. M. Geiger and D. J. Tobias, Molecular Orientation at the Squalene/Air Interface from Sum Frequency Generation Spectroscopy and Atomistic Modeling, *J. Phys. Chem. B*, 2021, **125**, 3932–3941.

73 H. Z. Zhang, Y. Q. Li, P. Davidovits, L. R. Williams, J. T. Jayne, C. E. Kolb and D. R. Worsnop, Uptake of gas-phase species by 1-octanol. 2. uptake of hydrogen halides and acetic acid as a function of relative humidity and temperature, *J. Phys. Chem. A*, 2003, **107**, 6398–6407.